

Strong Anisotropy of Dirac Cone in SrMnBi_2 and CaMnBi_2 Revealed by Angle-Resolved Photoemission Spectroscopy

Ya Feng¹, Chaoyu Chen¹, Youguo Shi¹, Zhuojin Xie¹, Hemian Yi¹, Aiji Liang¹,
Shaolong He¹, Junfeng He¹, Yingying Peng¹, Xu Liu¹, Yan Liu¹, Lin Zhao¹, Guodong
Liu¹, Xiaoli Dong¹, Jun Zhang¹, Chuangtian Chen², Zuyan Xu² and X. J. Zhou^{1,*}

¹*Beijing National Laboratory for Condensed Matter Physics,*

Institute of Physics, Chinese Academy of Sciences, Beijing 100190, China

²*Technical Institute of Physics and Chemistry,*

Chinese Academy of Sciences, Beijing 100190, China.

(Dated: December 01, 2013)

Abstract

We have provided direct evidence on the existence of strong anisotropic Dirac cones in SrMnBi_2 and CaMnBi_2 by carrying out high resolution angle-resolved photoemission measurements. In particular, we find distinct behaviors of the Dirac cone between SrMnBi_2 and CaMnBi_2 . In contrast to the band structure calculations, our measurements indicate that CaMnBi_2 is a new Dirac material exhibiting isolated Dirac cones with a giant anisotropy. These results prove the feasibility in engineering the Dirac cone anisotropy in the AMnBi_2 (A=Sr, Ca) system by manipulating the environment of the Bi square net and provide important electronic structure information in understanding its unusual properties.

The Dirac materials, so called because the behaviors of the low energy electrons in these materials can be described by the relativistic Dirac equation, have recently attracted much attention [1]. Such an interest is first triggered mainly by the discovery of graphene with its characteristic Dirac cones near the zone corner[2, 3]. The interest is further pushed to the full front by the discovery of the topological insulators with their characteristic Dirac cone in the topological surface state[4, 5]. The Dirac materials have expanded to encompass many other materials including the cuprate high temperature superconductors with a nodal Dirac cone in the *d*-wave superconducting state[6], the parent compound of the iron-based compounds[7, 8] and silicene[9–11]. Since the Dirac cone exhibits linear dispersion, massless and chiral low energy excitations[1], the Dirac materials exhibit a number of exotic and novel quantum phenomena including quantum Hall effect[12–15]. In addition to searching for new Dirac materials such as the three dimensional Dirac materials[16–20], a great effort has been devoted to engineer the Dirac cone. One particular aspect is to generate Dirac anisotropy because anisotropic Dirac transport can be harnessed for making new electronic devices when electrons propagate differently from one direction to the other. In contrast to graphene and the topological insulators where the Dirac cones are usually isotropic in momentum space, to generate Dirac anisotropy, various approaches have been proposed but have not yet been materialized, including patterned periodic potential[21] or strain[22], heterostructures[23, 24] and others[25, 26]. The AMnBi₂ (A=Sr or Ca) system has attracted special attention because it is expected that in this natural material, an anisotropic Dirac cone may be realized[27–31]. In particular, band structure calculations[27, 32] predict that the anisotropy of the Dirac cone in AMnBi₂ can be manipulated by local arrangement of Sr (or Ca) surrounding the Bi square net. This behavior, if proven true, will provide important information in understanding the origin of Dirac cone anisotropy and provide an ideal platform to tune the anisotropy of the Dirac cone.

Angle-resolved photoemission spectroscopy (ARPES) is a powerful tool which can directly reveal the presence of the Dirac cone and its anisotropy[33]. While there are some ARPES results for SrMnBi₂[27], so far no ARPES measurements have been reported for CaMnBi₂. In this Letter, we present high resolution angle-resolved photoemission results on both SrMnBi₂ and CaMnBi₂. We have revealed strongly anisotropic Dirac cones to experimentally prove that these two compounds are new members of bulk Dirac materials with anisotropic Dirac cones. We have found markedly different behavior of the Dirac cone between SrMnBi₂

and CaMnBi_2 . In particular, in contrast to the band structure calculations, we find that CaMnBi_2 is a Dirac material with isolated Dirac cones but with giant anisotropy. Indication of the spin-orbit coupling on the Dirac cone is also observed. These results prove the feasibility in engineering the Dirac cone anisotropy in the AMnBi_2 ($\text{A}=\text{Sr}, \text{Ca}$) system by manipulating the environment of the Bi square net[32] and provide important electronic structure information in understanding its unusual properties.

High quality single crystals of SrMnBi_2 and CaMnBi_2 with a typical dimension of $3\times 3\text{ mm}^2$ were grown by self-flux method. The ARPES measurements were carried out on our Lab photoemission system equipped with Scienta R4000 electron energy analyzer and Helium discharge lamp which gives a photon energy of $h\nu=21.218\text{ eV}$ [34]. The energy resolution was set at 20 meV and the angular resolution is ~ 0.3 degree. The Fermi level is referenced by measuring on the Fermi edge of a clean polycrystalline gold that is electrically connected to the sample. The crystals were cleaved *in situ* and measured in vacuum with a base pressure better than $5\times 10^{-11}\text{ Torr}$.

Figure 1 shows the constant-energy contours of SrMnBi_2 and CaMnBi_2 at different binding energies. The corresponding band structures of SrMnBi_2 and CaMnBi_2 are presented in Fig. 2 and Fig. 3, respectively. For SrMnBi_2 , there are two main features observed in the measured Fermi surface (Fig. 1c1). One is the weak square-shaped hole-like Fermi surface around Γ . The other is the four separated strong intensity segments in the first Brillouin zone that are confined along the Γ -M directions. Each segment grows in area with the increasing binding energy and gradually becomes a crescent moon-like shape (Fig. 1c2-c5). The Fermi surface of CaMnBi_2 (Fig. 1d1) exhibits similar features in that it also shows a hole-like square-shaped Fermi surface around Γ with a relatively strong intensity. But it shows a large diamond-like Fermi surface connecting four equivalent X points in the first Brillouin zone, different from the four isolated segments in SrMnBi_2 . With the increase of the binding energy, the portion of the large continuous contour near the Γ -M region also increases in area and forms four crescent moon-like pockets (Fig. 1d2-d5).

Figure 2 shows a detailed evolution of band structure with momentum in SrMnBi_2 . For each momentum cut, there are two sets of bands. One is a slightly broad inner band, denoted as IB in Fig. 2b for cut A, that gives rise to the square-shaped Fermi surface around Γ (Fig. 1c1). The other is an outer band, denoted as DB in Fig. 2b for cut A, that leads to the four strong-intensity segments in Fig. 1c1. The outer DB band consists of two sharp

linear bands, clearly observed for the momentum cuts A-F in Fig. 2a, as marked by the red dashed lines in Fig. 2b. The outer side of the DB linear band extends to high binding energy while the inner side becomes invisible when it merges with the inner IB bands. It is clear that the crossing point of the two DB linear bands is highest along the Γ -M direction (cut A) and lies above the Fermi level E_F for the cuts A, B and C (Fig. 2b). When the momentum cuts move away from the Γ -M direction, the energy position of the crossing point goes downwards and sinks to below E_F for the cuts D-F. We note that our results are different from the previous report where the Dirac point is below the Fermi level[27]. This difference may come from doping variation caused during the sample preparation. In order to quantitatively determine the location of the DB band crossing point in the momentum space and its corresponding energy, the two sides of the DB band are represented by two straight lines and the intersection points are taken as the band crossing position (dashed lines in Fig. 2b). The obtained momentum locus of the crossing points in SrMnBi_2 from different momentum cuts are shown in Fig. 4a and the variation of the crossing point energy along the locus is shown in Fig. 4c.

Figure 3 shows band structure evolution with momentum in CaMnBi_2 . It also consists of the inner IB bands and outer DB Dirac bands, as labeled in Fig. 3b for the cut C. However, the Dirac bands in CaMnBi_2 exhibit quite different behaviors from that in SrMnBi_2 . As seen from Fig. 3b, for the momentum cuts A and B near the Γ -M direction, the Dirac cone lies slightly above the Fermi level, which can be more clearly seen in the expanded view, cuts A'-B', of Fig. 3c. When the momentum cut moves away from the Γ -M direction, the DB band crossing point stays pinned close to the Fermi level for other momentum cuts C-G in Fig. 3b (expanded view in Fig. 3c for the cuts C' and D'). This is different from the continuous drop of the crossing point in SrMnBi_2 when the momentum moves away from the Γ -M direction (Fig. 2b). This difference in the Dirac band structure accounts well for the different topology of the resultant Fermi surface. Instead of four separated Dirac cones in the first Brillouin zone like four isolated islands for SrMnBi_2 (Fig. 1c1), the Dirac cones for CaMnBi_2 form a ridge-like topology that gives rise to a connected large diamond-like Fermi surface around Γ point (Fig. 1d1). The momentum locus of the crossing points in CaMnBi_2 is shown in Fig. 4b and the quantitative variation of the crossing point energy along the locus is shown in Fig. 4d.

We have revealed clear band asymmetry of the Dirac cone in SrMnBi_2 and CaMnBi_2 . As

seen in Fig. 2c for the cut G of SrMnBi₂, the Fermi velocity for the left-side linear band (10.9 eV·Å) is apparently steeper than that of the right-side one (2.4 eV·Å). Similar behavior is also seen in CaMnBi₂ where the Fermi velocity of the left and right-side bands of the Dirac cone (Fig. 3c, cut A') are 10.6 and 2.1 eV·Å, respectively. Band structure calculations have clearly shown that, with strong spin-orbit coupling introduced, the initially nearly symmetric Dirac band is expected to show velocity difference between the left and right sides, accompanied by an opening of a gap at the Dirac point[32]. Such a signature of strong spin-orbit coupling is clearly observed in SrMnBi₂ and CaMnBi₂ as manifested by the obvious Fermi velocity asymmetry between the left and right sides of the Dirac band.

Figure 4 shows the momentum locus of the crossing points obtained from different momentum cuts, their corresponding energy position along the locus and the Dirac band dispersion along the Γ -M direction. For both SrMnBi₂ and CaMnBi₂, since the Dirac point is above the Fermi level, we can not observe the upper branch of the Dirac cone and a possible gap opening near the Dirac cone due to the spin-orbit coupling[32]. We will therefore focus on the lower branch of the Dirac band. For SrMnBi₂, four isolated Dirac cones are observed in the first Brillouin zone that is consistent with the band structure calculations[32]. Along the Γ -M direction it shows a steep Dirac dispersion (thick black line in Fig. 4c), with a Fermi velocity of 10.9 eV·Å (left-side band). Along the momentum locus near the diagonal region (perpendicular to the Γ -M direction), the dispersion becomes rather flat, with a Fermi velocity of 0.59 eV·Å near the Dirac point. This gives a measured Dirac cone anisotropy of 18.5 that is slightly larger than the calculated value (~ 10)[32] and the previously reported value (~ 8)[27]. For CaMnBi₂, band structure calculations predict a continuous band crossing line with all the Dirac crossing points at the same energy[32]. However, our measurements clearly show that this is not the case because the drop of the crossing point is clear from cut A' to cut D' (Fig. 3c). This indicates that CaMnBi₂ still has isolated Dirac cones. However, CaMnBi₂ is unique in that the crossing point exhibits an initial slight drop from cut A to C, then levels off and stays at the similar energy position for the cuts C to G (Fig. 3). Along the Γ -M direction it shows a steep Dirac dispersion (thick green line in Fig. 4d) with a Fermi velocity of 10.6 eV·Å (left-side band). Along the momentum locus (perpendicular to the Γ -M direction), the dispersion becomes rather flat, with a Fermi velocity varying from 0.3 eV·Å near the diagonal region to nearly zero away from the diagonal region. This proves that CaMnBi₂ is a new Dirac material with isolated Dirac cones but with a giant Dirac

anisotropy.

Band structure calculations have shown that the Dirac cone in AMnBi_2 ($\text{A}=\text{Sr}$ or Ca) mainly originates from the A-Bi-A blocks in the crystal structure where the Bi square net is sandwiched between the upper and lower A layers (Figs. 1a and 1b)[27, 28, 32]. The Dirac bands come mainly from the Bi $p_{x,y}$ orbitals in the Bi square net which are weakly hybridized with Sr or Ca d orbitals. The introduction of A ions above and below the Bi square net doubles the initial unit cell to have two Bi atoms in the unit cell, causing band folding that gives rise to a continuous Dirac line. The particular arrangement of A ions leads to different Dirac cone behaviors between SrMnBi_2 and CaMnBi_2 [32]. In SrMnBi_2 , the Sr ions above and below the Bi square net are coincident (Fig. 1a), lifting the degeneracy on the Dirac line to form an isolated Dirac cone, which is consistent with our observation in SrMnBi_2 . On the other hand, in CaMnBi_2 , since the upper and the lower Ca ions are staggered (Fig. 1b), it is expected that the continuous Dirac line would be maintained[32]. While this qualitatively explains the larger Dirac cone anisotropy in CaMnBi_2 , it is not consistent with our observation of an isolated Dirac cone in CaMnBi_2 . To understand our results, further theoretical efforts are needed to introduce new factors that can generate anisotropic potential surrounding the Bi square net.

In summary, through high resolution ARPES measurements, we have provided direct experimental evidence that SrMnBi_2 and CaMnBi_2 are new Dirac materials with highly anisotropic Dirac cones. In particular, in contrast to the band structure calculations, we find that CaMnBi_2 is a new Dirac material with isolated Dirac cones but with giant Dirac anisotropy. We have revealed the dichotomy of the Dirac cone between SrMnBi_2 and CaMnBi_2 and the effect of the spin-orbit coupling on the Dirac cone structure. These results prove that the Bi square net in AMnBi_2 ($\text{A}=\text{Sr}$ and Ca) can provide an ideal platform from which, by tuning the surrounding environment, one can create and manipulate anisotropic Dirac cone[32]. Our results will also provide important information in understanding the unusual properties of the $(\text{Sr,Ca})\text{MnBi}_2$ system[27–31, 35].

We thank Zhijun Wang for discussions and his help in figure plotting. This work is supported by the National Natural Science Foundation of China (91021006, 10974239, 11174346 and 11274367) and the Ministry of Science and Technology of China (2011CB921703, 2013CB921700 and 2013CB921904).

*Corresponding author: XJZhou@aphy.iphy.ac.cn

- [1] O. Vafek and A. Vishwanath, arXiv:1306.2272.
- [2] K. S. Novoselov et al. Science **306**, 666 (2004).
- [3] A. H. Castro Neto, Rev. Mod. Phys. **81**, 109 (2009).
- [4] M. Z. Hasan and C. L. Kane, Rev. Mod. Phys. **82**, 3045 (2010).
- [5] X. L. Qi and S. C. Zhang, Rev. Mod. Phys. **83**, 1057 (2011).
- [6] J. Orenstein and A. J. Millis, Science **288**, 468 (2000).
- [7] G. D. Liu et al., Phys. Rev. B **80**, 134519 (2009).
- [8] P. Richard et al., Phys. Rev. Lett. **104**, 137001 (2010).
- [9] P. Vogt et al., Phys. Rev. Lett. **108**, 155501 (2012).
- [10] L. Chen et al., Phys. Rev. Lett. **109**, 056804 (2012).
- [11] B. J. Feng et al., Nano. Lett **12**, 3507 (2012).
- [12] K. S. Novoselov et al., Nature **438**, 197 (2005).
- [13] Y. B. Zhang et al., Nature **201**, 438 (2005).
- [14] M. I. Katsnelson et al., Nature Phys. **2**, 620 (2006).
- [15] M.I. Katsnelsona, K.S. Novoselovb, Solid State Commun. **143**, 3 (2007).
- [16] X. G. Wan, A. M. Turner, A. Vishwanath, S. Y. Savrasov, Phys. Rev. B **83**, 205101 (2011).
- [17] G. Xu et al., Phys. Rev. Lett. **107**, 186806 (2011).
- [18] A. A. Burkov, L. Balents, Phys. Rev. Lett. **107**, 127205 (2011).
- [19] Z. J. Wang et al., Phys. Rev. B **85**, 195320 (2012).
- [20] Z. J. Wang et al., Phys. Rev. B **88**, 125427 (2013).
- [21] C.-H. Park et al., Nature Phys. **4**, 213 (2008).
- [22] S.-M. Choi et al., Phys. Rev. B **81**, 081407 (2010).
- [23] V. Pardo and W. E. Pickett, Phys. Rev. Lett. **102**, 166803 (2009).
- [24] S. Banerjee et al., Phys. Rev. Lett. **103**, 016402 (2009).
- [25] G. E. Volovik, JETP Lett. **73**, 162 (2001)
- [26] P. Dietl et al., Phys. Rev. Lett. **100**, 236405 (2008).
- [27] J. Park et al. Phys. Rev. Lett. **107**, 126402 (2011).

- [28] J. K. Wang et al., Phys. Rev. B **84**, 064428 (2011).
- [29] K. F. Wang et al., Phys. Rev. B **84**, 220401(R) (2011).
- [30] K. F. Wang et al., Phys. Rev. B **85**, 041101(R) (2012).
- [31] J. B. He et al., Appl. Phys. Lett. **100**, 112405 (2012).
- [32] G. Lee et al. Phys. Rev. B **87**, 245104 (2013).
- [33] A. Damascelli et al., Rev. Modern Phys. **75**, 473 (2003).
- [34] G. D. Liu et al. Rev. Sci. Instrum. **79**, 023105 (2008).
- [35] K. F. Wang et al., App. Phys. Lett. **100**, 112111(2012).

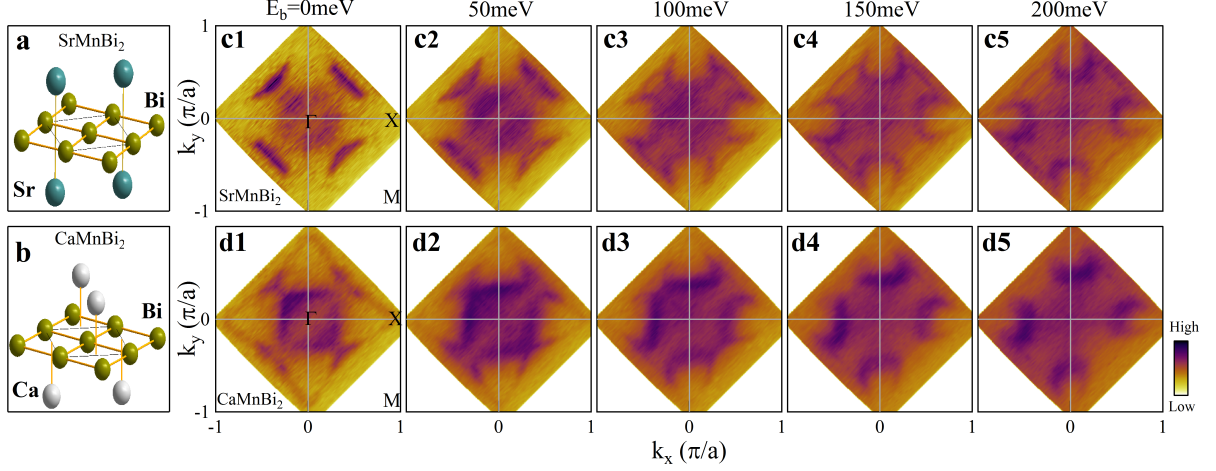


FIG. 1: Constant energy contours for SrMnBi_2 and CaMnBi_2 measured at 30 K. (a) and (b) show the Bi square net sandwiched between two Sr layers in SrMnBi_2 and two Ca layers in CaMnBi_2 in their crystal structures[32]. (c1-c5). Constant energy contours of SrMnBi_2 obtained by integrating the photoemission spectral weight over a 10 meV energy window with respect to the binding energy of 0 (c1), 50 meV (c2), 100 meV (c3), 150 meV (c4) and 200 meV (c5). The crystal structure of SrMnBi_2 is tetragonal with a space group of $I4/mmm$ and a lattice constant of $a=4.58 \text{ \AA}$ [32]. (d1-d5). Constant energy contours of CaMnBi_2 obtained by integrating the photoemission spectral weight over a 10 meV energy window with respect to the binding energy of 0 (d1), 50 meV (d2), 100 meV (d3), 150 meV (d4) and 200 meV (d5). The crystal structure of CaMnBi_2 is tetragonal with a space group of $P4/nmm$ and a lattice constant of $a=4.50 \text{ \AA}$ [32]. All the contours are obtained by symmetrizing the original data with respect to the $(\pi, -\pi)$ - $(-\pi, \pi)$ line.

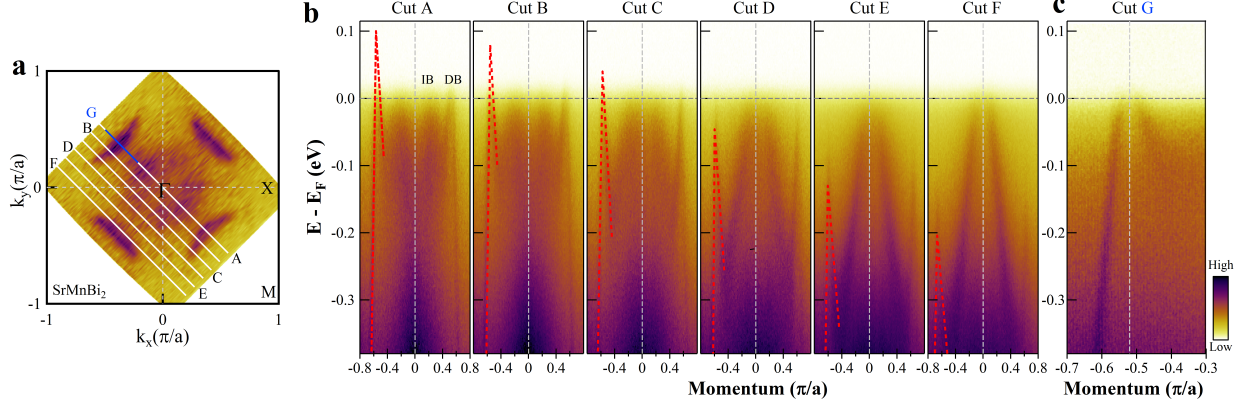


FIG. 2: Momentum dependence of the band structure in SrMnBi_2 . (a). Fermi surface of SrMnBi_2 measured at 30 K with the momentum cuts labeled. (b). Band structure along various momentum cuts labeled in (a) measured at 90 K. A relatively high temperature of 90 K is used here in order to see part of the bands above the Fermi level. Dashed red lines are drawn, as a guide to eyes, on top of one Dirac band on the left side of the images. (c) Expanded view of band structure to show the Fermi velocity asymmetry between the left-side and right-side of the Dirac band for cut G (blue line cut in (a)) along the Γ -M direction.

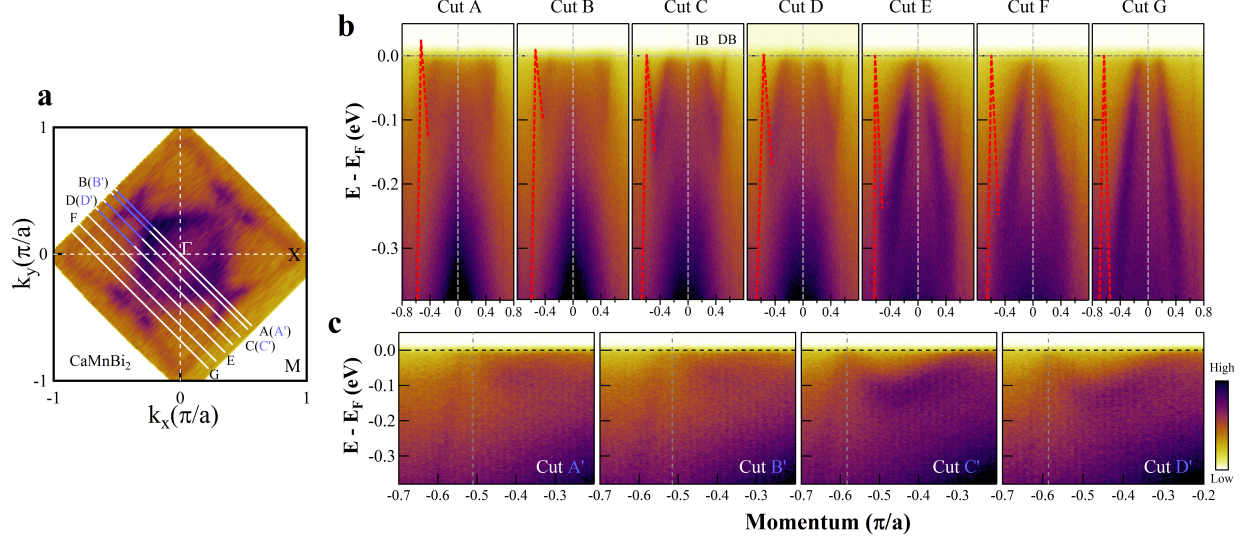


FIG. 3: Momentum dependence of the band structure in CaMnBi_2 . (a). Fermi surface of CaMnBi_2 measured at 30 K with the momentum cuts labeled. (b). Band structure along various momentum cuts labeled in (a) measured at 30 K. Dashed red lines are drawn, as a guide to eyes, on top of one Dirac band on the left side of the images. (c). Expanded images for the cuts A', B', C' and D' (blue line cuts in (a)) to see the location of the crossing points and the asymmetry between the left and right sides of the Dirac band.

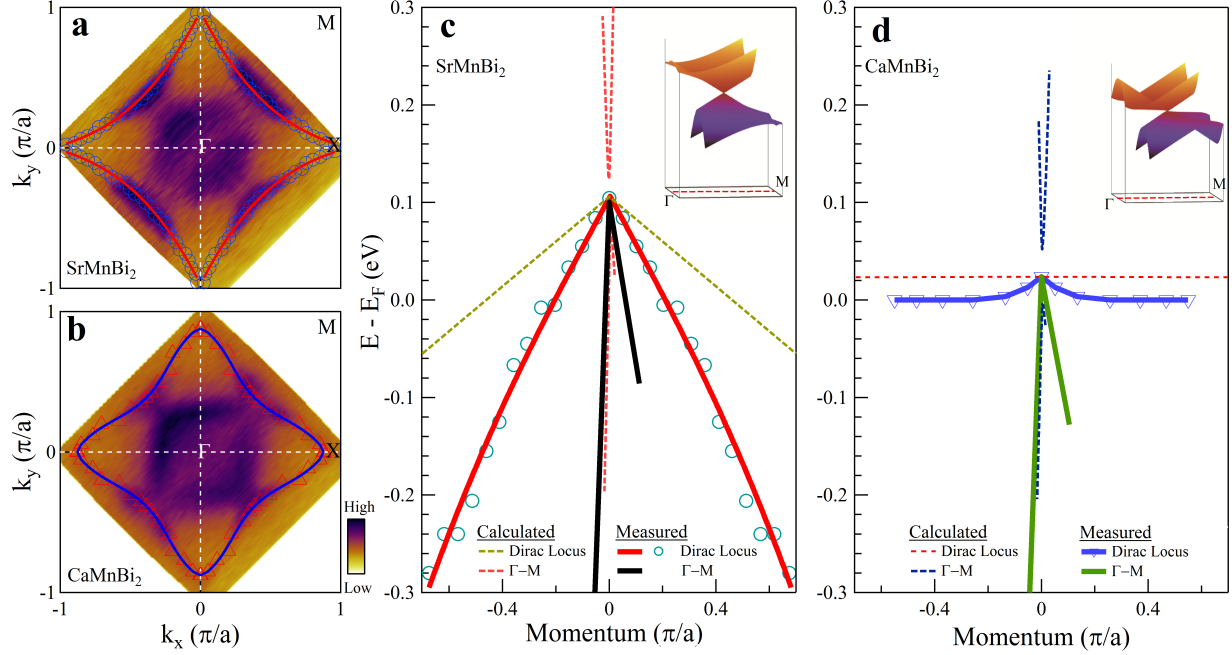


FIG. 4: Dichotomy of the Dirac cone anisotropy between SrMnBi₂ and CaMnBi₂. (a) and (b) show locus of the crossing points in the momentum space in SrMnBi₂ (blue empty circles) and CaMnBi₂ (red empty triangles), respectively. (c). Measured Dirac band dispersion along the Γ -M direction (thick black line) and momentum dependence of the crossing point energy along the underlying locus shown in (a) (red thick line) for SrMnBi₂. (d). Dirac band dispersion along the Γ -M direction (green thick line) and momentum dependence of the crossing point energy along the underlying locus shown in (b) (blue thick line) for CaMnBi₂. In (c) and (d), the calculated results (dashed lines) considering the spin-orbit coupling are also plotted for comparison[32]. The momentum value for the crossing point locus represents the integrated length along the locus curve with respect to the Dirac point along the Γ -M direction. The upper-right insets of (c) and (d) show a schematic of an anisotropic Dirac cone.